Original Article

Evaluation of Compton attenuation and photoelectric absorption coefficients by convolution of scattering and primary functions and counts ratio on energy spectra

Mansour Ashoor, Afrouz Asgari, Abdollah Khorshidi[1], Ali Rezaei

Department of Nuclear Imaging Systems, Radiation Application Research School, Nuclear Science and Technology Research Institute, [1]Department of Medical Physics and Biomedical Engineering, Tehran University of Medical Sciences, Tehran, Iran

ABSTRACT

Purpose: Estimation of Compton attenuation and the photoelectric absorption coefficients were explored at various depths. **Methods:** A new method was proposed for estimating the depth based on the convolution of two exponential functions, namely convolution of scattering and primary functions (CSPF), which the convolved result will conform to the photopeak region of energy spectrum with the variable energy-window widths (EWWs) and a theory on the scattering cross-section. The triple energy-windows (TEW) and extended triple energy-windows scatter correction (ETEW) methods were used to estimate the scattered and primary photons according to the energy spectra at various depths due to a better performance than the other methods in nuclear medicine. For this purpose, the energy spectra were employed, and a distinct phantom along with a technetium-99 m source was simulated by Monte Carlo method. **Results:** The simulated results indicate that the EWW, used to calculate the scattered and primary counts in terms of the integral operators on the functions, was proportional to the depth as an exponential function. The depth will be calculated by the combination of either TEW or ETEW and proposed method resulting in the distinct energy-window. The EWWs for primary photons were in good agreement with those of scattered photons at the same as depths. The average errors between these windows for both methods TEW, and ETEW were 7.25% and 6.03% at different depths, respectively. The EWW value for functions of scattered and primary photons was reduced by increasing the depth in the CSPF method. **Conclusions:** This coefficient may be an index for the scattering cross-section.

Keywords: Compton, convolution, depth, Monte Carlo method, photopeak

INTRODUCTION

Compton scattering is one of the most important processes on assessment interaction of radiation with material in which the ray will be attenuated quantitatively as Compton attenuation coefficient. This coefficient is a practical and applicable parameter for improving the images in nuclear medicine as well as decreasing the absorbed radiation dose along with the photoelectric absorption one. Also, each organ in the body is at a specific situation where acts the functional and physiological engagements in order to obtain health and high growth of cells. Every change in this spatial situation leads to appear abnormalities, lesions and loss of performance as well. Therefore, estimation of the organs' depth plays a key role in medicine due to providing helpful information for evaluating their performance, early diagnosis, as well as the better treatment. While those are deformed, the depth may be changed, and this can be probably utilized to detect the type and degree of disease. Clearly, the calculation of the depth depends on the peripheral tissues, the attenuation coefficient and the organ size that were considered in the existing methods.[1-7]

Nosil *et al.* employed two radioisotopes that their method was independent of the size, but assuming the attenuation coefficient of water to be constant.[3] On the other hand, Starck and Carlsson

Access this article online

Quick Response Code:

Website: www.ijnm.in

DOI: 10.4103/0972-3919.158532

Address for correspondence:
Dr. Abdollah Khorshidi, Department of Medical Physics and Biomedical Engineering, Tehran University of Medical Sciences, Tehran, Iran.
E-mail: abkhorshidi@yahoo.com

proposed a method in which the modulation transform function and the mean linear attenuation coefficient used, in contrast with depending size.[5] These methods were related to either the size or the total attenuation coefficient, as it has been done comparison of the methods on this matter, but all of them related to the other variable distinct parameters.

In this study, a new method proposed free from all aforementioned parameters in which convolution of the scattering and primary photons functions (CSPF) along with the triple energy-window (TEW) and extended triple energy-window (ETEW) methods is used for estimating depth of organs along with estimating Compton scattering attenuation coefficient and the photoelectric absorption coefficient using the energy spectra.

METHODS

The radiopharmaceutical, containing the nuclear materials, is used in order to evaluation of metabolic performance and physiological parameters of the tissues.[11,12] Due to the nature of nuclear radiation, several interactions between radiation and tissue occur according to different energies of the radiopharmaceutical. Photoelectric and Compton scattering are usually dominant phenomena in diagnostic nuclear medicine.[13] Although, the scattered gamma ray reduces image contrast,[14] but we have demonstrated that the depth can be found by this and some mathematical concepts, and then the Compton attenuation and the photoelectric absorption coefficients will be estimated.

Scatter estimation using triple energy-window

The TEW method,[8] has better performance than other methods in nuclear medicine,[9,10] and is based on the energy spectrum. The subtraction and trapezoidal laws are used in this method which the subtraction is carried out using two sets of data: One set is acquired with a main window centered at photopeak energy, and the other is acquired with two subwindows on both sides of the main window. The scattered photons (C_{scat}) included in the main window are estimated from the counts acquired with the subwindows and then they are subtracted from the count acquired with the main window. As shown in Figure 1, the count of primary photons (C_{prim}) is given by,[15]

$$C_{\text{prim}} = C_{\text{total}} - C_{\text{scat}} \quad (1)$$

The C_{scat} is estimated from the count data C_{left} and C_{right} acquired with the two subwindows that are located at both sides of the main window, as shown in Figure 2. Assuming that the width of the main window as W_m and that of the subwindow as W_s, the C_{scat} can be estimated from a trapezoidal region having a left height of C_{left}/W_s, a right height of C_{right}/W_s, and a base of W_m as follows:

$$C_{\text{scat}} \cong \left(\frac{C_{\text{left}}}{W_s} + \frac{C_{\text{right}}}{W_s} \right) W_m / 2 \quad (2)$$

The C_{prim} can be calculated using Eqs. (1, 2). The choice of the energy-window width (EWW) for the values of W_m and W_ss is critical in these methods because the accuracy is related severely to the EWW value and the detector system. The photopeak point has spatial shift more to the left side on the spectrum when the C_{scat} is increased. This shift may also be considered as a preliminary estimation of the C_{scat} which this is beyond the scope of this study, and it is not considered at accounting process here. This matter may be an error source in CSPF method.[16]

Scatter estimation using extended triple energy-window

Bong *et al.* proposed this method in order to improve the quality of the nuclear medicine images.[17] The ETEW method estimates scatter counts with the trapezoidal approximation as follows,

$$C_s = \left(\frac{C_{\text{left}}}{W_{\text{left}}} - \frac{C_{\text{right}}}{W_{\text{right}}} \right) (W_1 + W_2) \frac{W_m}{2W} + \frac{C_{\text{right}}}{W_{\text{right}}} W_m \quad (3)$$

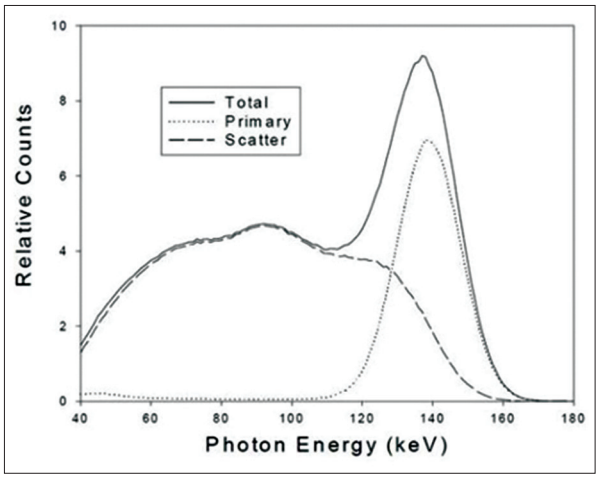

Figure 1: The simulated total, primary, and scatter energy spectra with technetium-99m in phantom

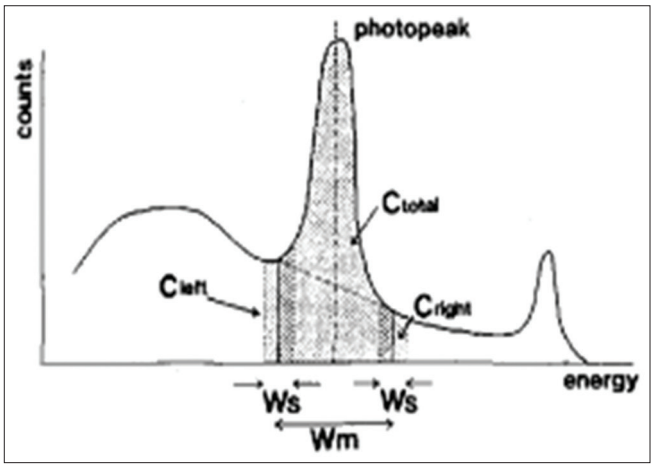

Figure 2: The energy spectrum used at the triple energy-windows method for estimating the scattered and primary counts along with the chosen energy-windows

Where W is difference between the centers of the right and left subwindows, W_1 is difference between the center of the right subwindow and lower bound of the main window, and W_2 is difference between the center of the right subwindow and upper bound of the main window, as shown in Figure 3.

Convolved scatter and primary functions method

The aim was to present a new method for calculating the organ depth independent of the linear attenuation coefficient. Estimation of the depth is useful for measuring the amount of radioactive tracker taken up by an organ in the body. This method is based on the mathematical relations as convolution of two exponential functions that both the related parameters of these functions and its result mapping on the spectrum curve which they were determined by the Monte Carlo method and Matlab software. Obviously, the convolution operator is the effectiveness of a function on the other function with progressing some known variables. In the interaction of radiation with matter, the energy value is decreased gradually, and it seems that these energies will act together totally on the system so that one may consider the CSPF appeared in the energy spectrum. However, the spectrum is a final result from these interactions. In CSPF method, two pseudo-analogical expressions are introduced on the spectra. The first, the spectrum function (C (E)) is the convolution of two exponential functions, and the second, the scattered (C_s (E)) and primary (C_p (E)) photon functions are as exponential functions, as indicated in Figure 4 in which the origin of coordinates is metaphorical. One may obtain the function of C (E) as follows,

$$C(E) = C_S(E) \circledast C_P(E) = \varphi e^{-\alpha E} \circledast \omega e^{-\beta E} = \frac{\varphi\omega}{\beta-\alpha}\left(e^{-\alpha E} - e^{-\beta E}\right) \quad (4)$$

Where α, β and ω are the constant parameters, which are determined by the some distinct points on the spectrum curve using Matlab software (MathWorks, Inc., 3 Apple Hill Drive, Natick, MA 01760-2098 USA). The C_{scat} and C_{prim} are calculated by the TEW and ETEW methods at various depths. In this method, these values are the integrand of the C_s (E) and C_p (E) functions over the ΔE_{CS} and ΔE_{CP} windows as follows,

$$C_{Scat} = \int C_s(E)\,dE = \int_{140-0.5\Delta E_{CS}}^{140+0.5\Delta E_{CS}} \varphi e^{-\alpha E}\,dE \quad (5)$$

$$C_{Scat} = \int C_s(E)\,dE = \int_{140-0.5\Delta E_{CP}}^{140+0.5\Delta E_{CP}} \omega e^{-\beta E}\,dE \quad (6)$$

The energies are in terms of keV and the technetium-99m (Tc-99m) source has 140-keV gamma ray. The ΔE_{CS} and ΔE_{CP} values will be calculated from the energy spectra at different depths by solving the Eqs. (5, 6) using Matlab software. The distance from the detector, namely depth (d), is related to the energy-windows of ΔE_{CS} and ΔE_{CP} as follows,

$$\Delta E_{CS} \cong \Delta E_{CP} = \sigma e^{-\tau \times d} \quad (7)$$

The aim is the determination of the σ and τ unknown parameters. Therefore, one may estimate the depth value using Eq. (7) in which the energy-window calculated by both the ETEW and CSPF methods on the energy spectrum obtained in nuclear imaging with applying the flowchart as indicated in Figure 5. This flowchart shows the step by step for the calculation of these unknown parameters. Finally, with characterizing Eq. (7), one the first obtains the spectrum and procedures for determining the ΔE_{CS} or ΔE_{CP} values, and then the depth will be determined.

Determination of the Compton attenuation coefficient

The second, the relationship between the counts ratio and the Compton attenuation coefficient has been evaluated. The radiopharmaceuticals concentrated in the special organs may be considered as the volumetric sources along with a special pharmaceutical signal to noise ratio (S/N) in which the rays employed to determine the anatomical and functional parameters. For instance, a Tc-99m point source is positioned beyond an attenuator that decreases both the number and energy of the rays at the different situations, as shown in Figure 6. Some of the rays can pass through the material without scattering to be recorded under the photopeak region. The ray on the straight path does not react with the matter that will pass from the hole of collimator and will reach into the detector. With regard to the resolution and related parameters on the detection, the rays will be detected and recorded under the photopeak region on the energy spectrum. In contrast, the ray passing through the attenuator with the small angle (θ) relative to normal line interacts at the distance of x from the source at the dx thickness included in the attenuator due to its Compton attenuation coefficient that will be scattered so that Compton phenomenon will act as priority one. The scattered photon will travel through the distance of L and will be recorded in the Compton region on the spectrum. The primary counts (C_p) has been calculated by,

$$C_{prim} = kI_0 e^{-\mu d} \quad (8)$$

Where k, I_0, and μ are the buildup factor along with the other parameters of the detector, the primary intensity of the source, and total linear attenuation coefficient, respectively. To estimate theoretically the number of the scattered photons recorded in the Compton region of the spectrum, a thickness of dx away from a distance of x from the source is considered. The number of descending photons to this thickness is as follows,

$$k' I_0 e^{-\mu x} \quad (9)$$

That the number of the scattered photons with respect to the Compton scattering attenuation coefficient (μ_{sc}) and the thickness of dx is as follows,

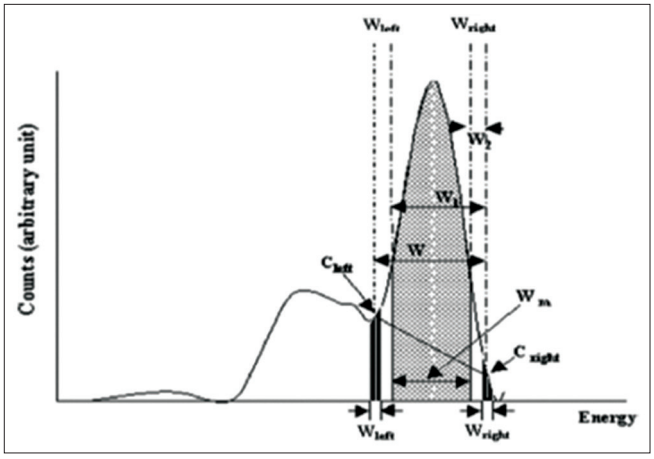

Figure 3: The energy spectrum used at the extended triple energy-windows scatter correction method for estimating the scattered and primary counts along with the chosen energy-windows

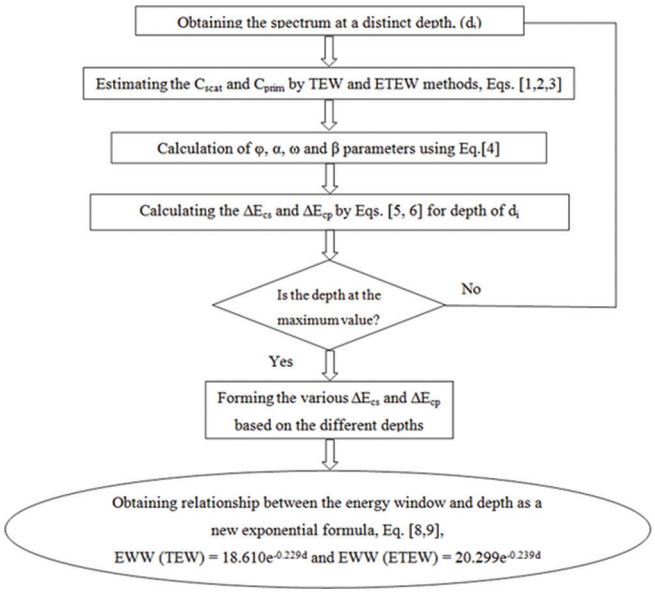

Figure 5: Flowchart of implementation of the proposed method

$$k' I_0 e^{-\mu x} \times \mu_{sc} \times dx \tag{10}$$

After the attenuation process, the fraction of these photons detected by the detector will be as follows,

$$k' I_0 e^{-\mu x} \times \mu_{sc} \times dx \times e^{-\mu l} \tag{11}$$

Where K' is the same as K, but without considering parameters of the detector. Regarding to be small angle of θ less than 5° (θ <5°), one may obtain the following approximation,

$$l \cong d - x \tag{12}$$

That it is true. Therefore, the number of the scattered photons (dC_s) at the thickness of dx will be calculated as follows,

$$dC_s = k' I_0 e^{-\mu x} \times \mu_{sc} \times dx \times e^{-\mu(d-x)} = k' I_0 e^{-\mu d} \times \mu_{sc} \times dx \tag{13}$$

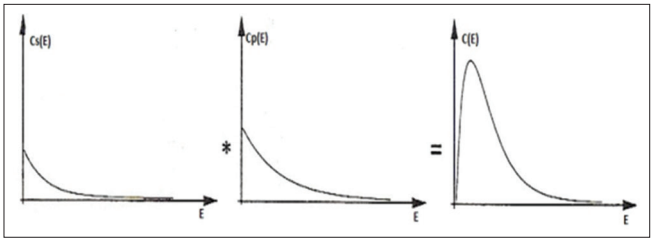

Figure 4: Convolution of two exponential functions

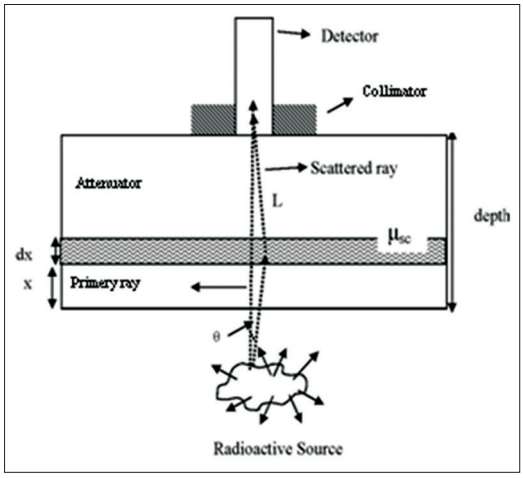

Figure 6: Schematic of presentation for calculation of the Compton attenuation coefficient

Because there is a probability of gamma ray interaction and scattering process in the total distance (d), for computing the total number of the scattered photons (C_s) in the thickness of d, one may obtain an integration on the distance from 0 to d as follows,

$$C_s = \int_0^d dC_s = k' I_0 e^{-\mu d} \times \mu_{sc} \times d \tag{14}$$

By dividing the Eq. (14) to (8), it is shown that the ratio of the number of scattered to primary photons is proportional to the d and μ_{sc} as follows,

$$\frac{C_s}{C_p} = \frac{k' I_0 e^{-\mu d} \times \mu_{sc} \times d}{k' I_0 e^{-\mu d}} = \frac{k'}{k} \times \mu_{sc} \times d \tag{15}$$

Where the k, k are assumed as invariable and constant values. Finally, one may estimate the μ_{sc} as follows,

$$\mu_{sc} \cong \kappa' / \kappa \times \frac{C_s / C_p}{d} \tag{16}$$

Therefore, the μ_{sc} is proportional to the scattered/primary ratio, and inversely with the depth.

Simulation method and computation of the parameters

To study the effects of interactions, Monte Carlo N-Particle version 4C (MCNP4C) code was used here. The input files

would specify geometry of source objects, collimators and detector planes for a distinct aim, which input files and geometry specifications are often complex and can be very cumbersome.[18,19] This code was modified to simulate spectra from phantom including the Tc-99m source. The NaI (Tl) crystal with the size of 39 cm × 39 cm, the thickness of 0.9525 cm and a low energy general purpose collimator with the parallel hexagonal holes at the size of 0.145 cm of small diameter, 0.02 cm inter-hole spacing, and 2.41 cm thickness are used in simulation as shown in Table 1.

The phantom is a cylinder, the diameter of 20 cm and the height of 30 cm, full of water placed at the front of the detector, and the spherical source with 2-cm diameter was inserted at distance of 5 cm from the center of the cylinder and 5 cm from the detector, as shown in Figure 7, then it was prepared for MCNP4C code input, which it run by F8 tally (energy distribution of pulses created in the detector as pulse height). The trajectories of 10^9 photons for the phantom were calculated using the workstation. The validity of the simulation was also confirmed with a spectrum of a distinct source.

The detector is to be closed to the phantom for improving signal to noise ratio (SNR). Source is placed at distances of 1 cm through 20 cm from the detector. The depths were calculated relying on energy spectra taken from MCNP4C code.

RESULTS

The response of the detector is simulated with the F8 tally and E8 card. For instance, the output file from the modified code for geometric shape is shown in Figure 8. The obtained spectra in each depth are shown in Figure 9. The Compton scattering counts at the depths <4 cm are similar together because of the concept of mean free path value at which the attenuation coefficient of water plays a key role. In contrast, the primary counts were decreased with increasing depths. When the depth is increased, the ratio of scattered to primary counts will be increased.

Table 1: Geometric characteristics of parallel beam collimator (in terms of cm)

Collimator	Parallel
Hole shape	Hexagonal
Central hole length	2.41
Hole size	0.145
Septal width	0.02

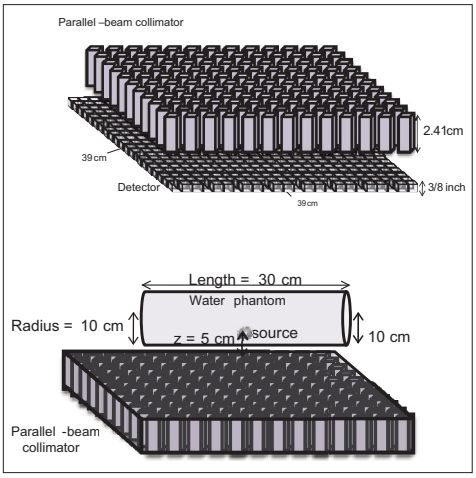

Figure 7: Parallel Beam collimator with hexagonal holes and point source in scatter medium in front of collimator at z (depth) = 5 cm

The simulated values of photopeak point (C_m, E_{Cm}), 2/3 of its point ($2/3C_m$, $E_2/_3C_m$), and ϕ by the Compton edge valley on the energy spectrum were calculated for estimating the α, β and ω parameters. These parameters used for calculating the C_p and C_s functions were determined from Eqs. (2,3) These calculated parameters at various depths are indicated in Table 2. The amounts of scattered and primary photons were measured at various depths by the TEW and ETEW methods in the phantom. We used a main window (W_m: 126–154 keV [20% of 140 keV]) and subwindows (Ws: 3 keV centered at 126 and 154keV) on the simulated spectrum in TEW method, and a main window (W_m: 126–154 keV [20% of 140 keV]) and subwindows (Ws: 3 keV centered at 123.5 and 156.5 keV) in ETEW method. The widths of the energy-windows (ΔE_{CP} and ΔE_{CS}) were calculated using the Table 2 and Eqs. (4, 5), as shown in Table 3. The EWWs for primary photons are in good agreement with those of scattered photons in the CSPF method. The average error between these windows for TEW and ETEW methods were 7.25% and 6.03% at all depths, respectively. Therefore, we may use the EWW of scattering instead of that of primary and vice versa.

The EWW value for functions of scattered and primary photons is reduced by increasing the depth in the CSPF method, as indicated in Figure 10. The EWWs at different depths were fitted by the exponential curve as follows,

$$EWW = 18.610e^{-0.229d}, \text{ for TEW method} \quad (17)$$

$$EWW = 20.299e^{-0.239d}, \text{ for ETEW method} \quad (18)$$

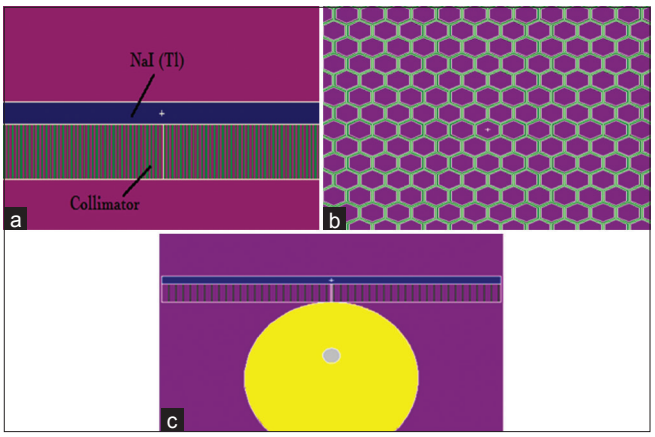

Figure 8: A schematic representation of the simulated gamma camera, (a) collimator with the parallel hexagonal holes, (b) and phantom and detector (c)

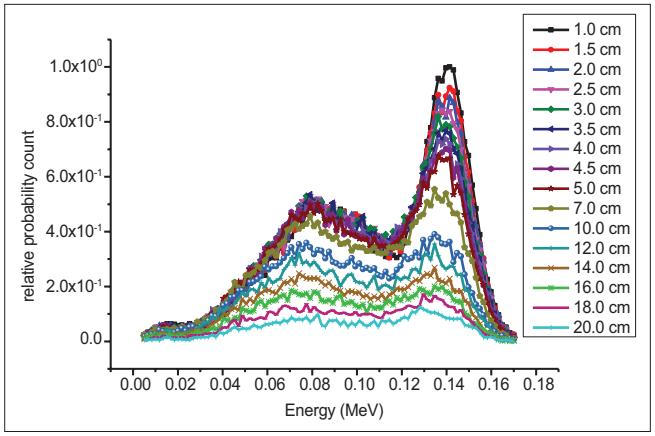

Figure 9: The simulated energy spectra at different depths

At $d = 0$, the EWW may be a criterion for detector performance, and the simulated spectrum is shown in Figure 11. The more the EWW, the less energy resolution of the detector will be.

As shown in Figures 12 and 13, the scattered to primary counts ratio as a linear function of depth are determined as $C_s/C_p = 0.1122\ d + 1.4235$ ($R^2 = 0.9130$) at the TEW method, and as $C_s/C_p = 0.1140\ d + 0.9079$ ($R^2 = 0.9517$) at the ETEW method using data in Table 3. The Compton attenuation coefficients were 0.1122 and 0.1140 cm^{-1} for these methods for Tc-99m in water phantom, respectively. The total attenuation coefficient for this state was 0.15 cm^{-1} so that the photoelectric absorption coefficient was 0.0378 and 0.0360 for TEW and ETEW methods, respectively.

DISCUSSION

In this study, the μ_{sc} and the depth were investigated by new methods along with reputable proposed assumptions using Monte Carlo method. As known, the choice of energy-window at the energy spectra is important for the SNR and image contrast. We have demonstrated that the EWW is proportional to the depth with respect to the primary and scattered photon counts. While the energy spectra obtained both as experimentally by the detector systems and as theoretically either by the simulation using the Monte Carlo method or the calculation by the existing formulas are accessible, one may extract the more information on tracer, detector system, and the geometrical specifications of organ.

The TEW and ETEW methods have been used for estimating the scattered and primary counts accurately. Though the spectra of the scattered photons vary with object size, source distribution, and source energy, estimation of the scattered photons as a trapezoid is good approximation. The other problem is the energy value used in the field of imaging that leads to appearing the Compton scattering and photoelectric absorption processes. Emitted gamma radiation interacts with the body based on these processes, producing a significant attenuation in the primary beam at energies. These mechanisms are well known, and those were a basis in our method.

Table 2: The calculated parameters on the spectrum by MCNP4C code

Depth (cm)	C_m (10^{-7})	(2/3)×C_m (10^{-7})	E_{cm} (KeV)	E (right)$_{(2/3)\ Cm}$ (KeV)	E (left)$_{(2/3)\ Cm}$ (KeV)	φ*(10^{-3})	ω	α	β
1	12.612818	8.408545	140.9361	149.9311	129.7891	5.839333	0.00583231490552	19.3388883933362510	19.3388883933363831
3	10.352648	6.901766	137.0196	149.5868	127.7666	5.014925	0.00413652351014	12.5692097925346672	12.5692097253797O
5	8.5513608	5.700907	136.2879	148.3818	123.2042	4.640035	0.00285673440931	9.5993833795864500	9.5993833795864500
7	7.0223881	4.681592	135.6955	147.9945	123.3764	4.298507	0.00210957972823	7.7513744365590550	7.7513744365520780
10	4.9187884	3.279193	135.0828	147.6071	117.9535	3.166374	0.00124737823486	0.4762239918395510	0.4762239918007220
12	4.3819140	2.921276	135.0297	147.2628	122.0422	2.604916	0.00115658300141	−1.9006660737391310	−1.9006660737399900
14	3.3929610	2.261974	135.8145	147.0881	113.7155	2.173178	0.00087866983899	−5.8851205987320960	−5.8851205984553610
16	2.5261194	1.691103	135.212	147.0058	112.0572	1.704400	0.00060942864337	−8.1044156110852780	−8.1044156107964120
18	2.1764706	1.450980	129.7461	144.2070	107.351	1.267047	0.00051274102256	−8.4254359730395730	−8.4254359713815830
20	1.5798946	1.053263	128.6271	143.9151	106.2167	1.204975	0.00040778763746	−8.7367905193976410	−8.7367905183449130

*φ=C_{edge}×10^4. MCNP4C: Monte Carlo N-Particle version 4C

Table 3: The calculated scattered and primary photons, EWWs and relative error at both methods

Depth (cm)	TEW method						ETEW method					
	$C_p(10^{-6})$	$C_s(10^{-6})$	$C_t(10^{-6})$	ΔE_{CP} (KeV)	ΔE_{CS} (KeV)	Relative error (ΔE_{CP}, ΔE_{CS}) (%)	$C_p(10^{-6})$	$C_s(10^{-6})$	$C_t(10^{-6})$	ΔE_{CP} (KeV)	ΔE_{CS} (KeV)	Relative error (ΔE_{CP}, ΔE_{CS}) (%)
1	6.925396	9.398694	16.324100	19.714	20.114	1.99	8.870679	7.453320	16.32400	21.600	20.000	8.00
3	4.781002	8.722003	13.503010	9.852	10.098	2.44	6.306530	7.196470	13.503010	8.800	8.400	4.50
5	3.824005	7.003999	10.82800	5.234	5.800	9.75	4.352830	6.776170	11.129000	5.800	5.600	3.45
7	2.888701	6.225397	9.114098	4.052	4.286	5.46	3.206140	5.907860	9.113997	4.200	4.000	5.00
10	1.706300	4.596704	6.303004	1.462	1.518	3.69	1.847510	4.455490	6.303004	1.583	1.504	5.26
12	1.213000	3.835999	5.048999	0.924	1.008	8.34	1.579250	3.585750	5.164999	1.046	1.055	0.81
14	0.919701	3.005395	3.925096	0.559	0.606	7.75	1.131600	2.777840	3.909440	0.565	0.561	0.71
16	0.754297	2.384705	3.139002	0.398	0.449	11.35	0.804211	2.040790	2.845001	0.424	0.385	9.19
18	0.585696	1.801300	2.386995	0.389	0.351	9.77	0.501870	1.444130	1.946000	0.301	0.350	14.00
20	0.344994	1.241997	1.586991	0.283	0.249	12.01	0.311840	1.008160	1.320000	0.225	0.246	9.34

EWWs: Energy-window widths, TWE: Triple energy-window, ETEW: Extended triple energy-windows

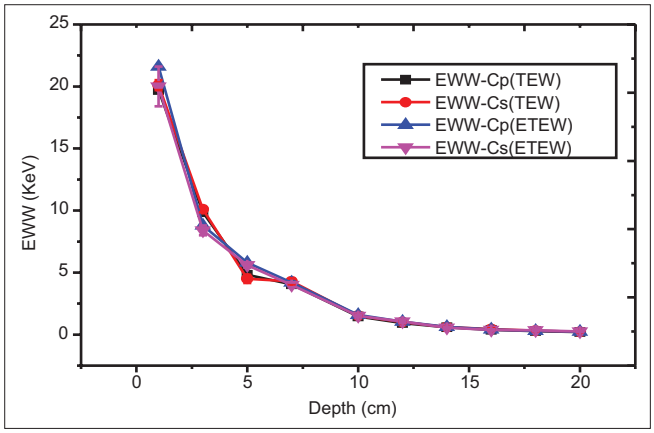

Figure 10: The energy-window width values as function of depth for the scattered and primary counts at the extended triple energy-windows methods

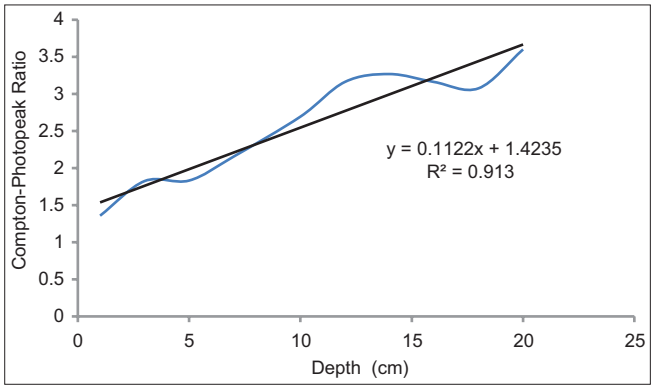

Figure 12: The scattered to primary counts ratio as a linear function of depth at the triple energy-windows method

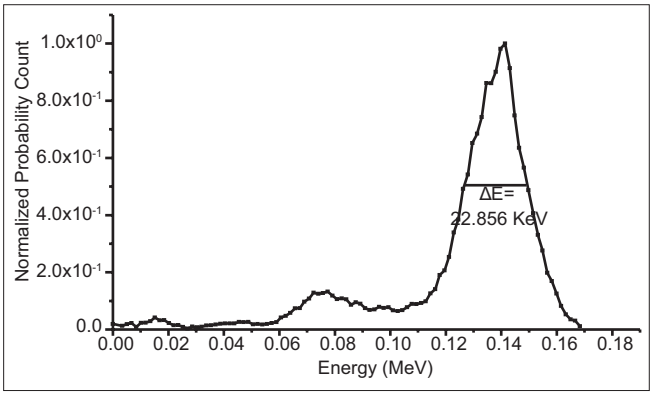

Figure 11: The simulated energy spectrum at zero depth (without phantom)

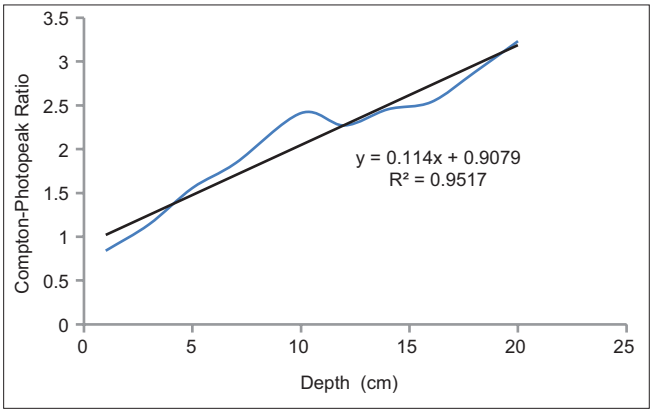

Figure 13: The scattered to primary counts ratio as a linear function of depth at the extended triple energy-windows scatter correction method

The simulated results indicate that the EWW value is decreased with increasing depth due to the more attenuation and higher cross-sections. It is found that the relationship between the EWW and depth is as exponential function. This method may be used for estimating energy resolution of detector system. Also, it is estimated a distinct distance that Compton scattering regions at depths lower than this distance (4 cm) are similar to with each other. This distinct depth is probably useful to better compensation of scattering for organs close to the skin.

The scattered photons of the photopeak window are mainly contributed by the first-order Compton scatter.[20] The Compton scattering which may be identified by the cross-sections that will vary with the energy of gamma ray has a key role in this study, although in the field of imaging is unsuitable and must be compensated in order to having a better diagnosis. The C_{scat} value is important both to improve SNR and to estimate depth because the increase in SNR and the reduction of noise followed by the rejection of scattering that it can be clearly observed as well as to provide better quality in the reconstructed images.[21]

Corrections for scattering are necessary in order to obtain the higher quantitation accuracy,[22-41] which at all categories, the depth parameter is not considered. It can be used to compensate some effects due to scattering that is undesirable for forming a qualified image. Also, it seems that the noise is an important factor to accuracy estimation of depth as well as the rigid and flexible motions. To decrease these effects, it must be prepared some methods before obtaining the spectra. Some theoretical formulas could be used to rapidly assess the impact of different scatter correction strategies on image quality.[42]

Several methods for the effects of scattered events have been proposed.[38-49] The difference between methods is the way of estimating the scatter contribution. As known, the TEW and ETEW methods can directly calculate the scattered photons in the main window using the subwindows that are located at both sides of the main window, the scatter component corresponds to the source position and the shape of the scatterer, the localization of the source distribution is considered as well as the shape of the scatterer. The errors in estimating scattered photons are due to the center location of the subwindows, which are defined on both sides of the main window. Scattered fractions were estimated correctly within an 8% error using the 26% window and within a 10% error using the 20% window. When we select a 2–6 KeV subwindow, the scatter correction can perform well for this phantom.[17] In the actual gamma camera system, however, the determination of the optimum location of the center and the width of the subwindow should be based on the results of experiment because the system may differ from the simulation model in the stability of gain and other factors.

One can estimate the count ratios of the subwindows to the main window. From this result, if the radionuclide that has a single photopeak is measured using narrow subwindows and a large main window, the measured counts of the right subwindow will be <5% of the main window. Therefore, the counts of the high-energy subwindow (C_{right}) may be insignificant for the radionuclide, and then one can set the count C_{right} to zero. However, for a radionuclide having multiple photopeaks, or for a combination of radionuclides, the count (C_{right}) may not always be insignificant. In clinical cases, it is difficult to get energy spectra at pixels with good statistics.

The μ_{sc} is a fraction of total attenuation coefficient indicating only the Compton cross-section in a distinct substance. This parameter will be varied with the impurities, crack and cleavages existing in substance. The lower the μ_{sc}, the more stable the C_s/C_P value, thus the effect of the depth value will be insignificant. While the μ_{sc} is increased, this ratio will be unstable in each depth. The advantage of estimating the μ_{sc} is for better compensation of scattered counts in images with forming the μ_{sc}-map.

CONCLUSIONS

The primary and scattered counts were calculated by TEW and ETEW methods at the various depths, and then the data extracted from these methods were applied in the CSPF method. As a result, the EWW was obtained at each depth. The widths of energy-window calculated with primary photons were in good agreement with those of scattered photons.

REFERENCES

1. Koral KF, Johnston AR. Estimation of organ depth by gamma ray spectral comparison. Phys Med Biol 1977;22:988-93.
2. Koral F, Johnston AR. Effect of noise, order and range in fitting the photopeak region of local, Anger-camera energy spectra. Nucl Instrum Methods Phys Res 1990;299A: 548-53.
3. Nosil J, Sethi V, Bland J, Kloiber R. Double peak attenuation method for estimating organ location. Phys Med Biol 1987;32:1407-16.
4. Almén A, Nilsson M. Simple methods for the estimation of dose distributions, organ doses and energy imparted in paediatric radiology. Phys Med Biol 1996;41:1093-105.
5. Starck SA, Carlsson S. The determination of the effective attenuation coefficient from effective organ depth and modulation transfer function in gamma camera imaging. Phys Med Biol 1997;42:1957-64.
6. Egbert SD, May RS. A spectral unfolding method to determine source depth distribution. Phys Med Biol 1980;25:453-61.
7. Filipow LJ, Macey DJ, Munro TR. The measurement of the depth of a point source of a radioisotope from gamma ray spectra. Phys Med Biol 1979;24:341-52.
8. Ogawa K, Harata Y, Ichihara T, Kubo A, Hashimoto S. A practical method for position-dependent Compton-scatter correction in single photon emission CT. IEEE Trans Med Imaging 1991;10:408-12.
9. Perisinakis K, Karkavitsas N, Damilakis J, Gourtsoyiannis N. Effect of dual and triple energy window scatter correction methods on image quality in liver scintigraphy. Nuklearmedizin 1998;37:239-44.
10. Hayashi M, Deguchi J, Utsunomiya K, Yamada M, Komori T, Takeuchi M, *et al.* Comparison of methods of attenuation and scatter correction in brain perfusion SPECT. J Nucl Med Technol 2005;33:224-9.
11. Bihl GR, Bird NJ, Peters C, Bradley JR, Peters AM. Radionuclide method for evaluating the performance of hemodialysis *in vivo*. Kidney Int 2005;67:721-31.
12. Dai X, Chen Z, Tian J. Performance evaluation of kinetic parameter estimation methods in dynamic FDG-PET studies. Nucl Med Commun 2011;32:4-16.
13. Bushberg JT, Boone JM. The Essential Physics of Medical Imaging. 4th ed.. New York: Williwms and Wilkins; 2012.
14. King M, Farncombe T. An overview of attenuation and scatter correction of planar and SPECT data for dosimetry studies. Cancer Biother Radiopharm 2003;18:181-90.
15. King MA, Glick SJ, Pretorius PH, Wells RG, Gifford HC, Narayanan MV, *et al.* Attenuation, scatter and spatial resolution compensation in SPECT. In: Wernick MN, Aarsvold JN, editors. Emission Tomography: The Fundamentals of PET and SPECT. Worcester, Massachusetts: Academic Press; 2005.
16. Asl MN, Sadremomtaz A, Bitarafan-Rajabi A. Evaluation of six scatter correction methods based on spectral analysis in (99m) Tc SPECT imaging using SIMIND Monte Carlo simulation. J Med Phys 2013;38:189-97.
17. Bong J, Son H, Doo Lee J. Improved scatter correction for SPECT images: A Monte Carlo study. IEEE Trans Nucl Sci 2005;52:1263-70.
18. Yancht JC, Dobrzenieckit AB, Ramanathant C, Behrmanl R. Physically realistic Monte Carlo simulation of source, collimator and tomographic data acquisition for emission computed tomography. Phys Med Biol 1992;37:853-70.
19. Briesmeister JF. MCNP Data Manual. Los Alamos, New Mexico: Los Alamos National Laboratory; 2001.
20. Koral KF, Swailem FM, Buchbinder S, Clinthorne NH, Rogers WL, Tsui BM. SPECT dual-energy-window Compton correction: Scatter multiplier required for quantification. J Nucl Med 1990;31:90-8.
21. Sakelliosa NG, Karalia E, Lazarob D, Loudosa GK, Nikitaa KS. Monte-Carlo simulation for scatter correction compensation studies in SPECT imaging using GATE software package. Nucl Instrum Methods Phys Res 2006;569:404-8.
22. Jaszczak RJ, Greer KL, Floyd CE Jr, Harris CC, Coleman RE. Improved

SPECT quantification using compensation for scattered photons. J Nucl Med 1984;25:893-900.
23. Cho ZH, Jones JP, Singh M. Foundations of Medical Imaging. Los Angeles, California: John Wiley and Sons, Inc.; 1993. p. 176.
24. Axelsson B, Msaki P, Israelsson A. Subtraction of Compton-scattered photons in single-photon emission computerized tomography. J Nucl Med 1984;25:490-4.
25. Floyd CE Jr, Jaszczak RJ, Greer KL, Coleman RE. Deconvolution of Compton scatter in SPECT. J Nucl Med 1985;26:403-8.
26. Todd-Pokropek AE, Clarke G, Marsh R. Preprocessing of SPECT Data as a Precursor for Attenuation Correction. Information Processing in Medical Imaging. Information Processing in Medical Imaging; 1984. p. 130-50.
27. Msaki P, Axelsson B, Larsson SA. Some physical factors influencing the accuracy of convolution scatter correction in SPECT. Phys Med Biol 1989;34:283-98.
28. Jaszczak RJ, Floyd CE, Coleman RE. Scatter compensation techniques for SPECT. IEEE Trans Nucl 1985;32:786-93.
29. Beekman FJ, Kamphuis C, King MA, van Rijk PP, Viergever MA. Improvement of image resolution and quantitative accuracy in clinical Single Photon Emission Computed Tomography. Comput Med Imaging Graph 2001;25:135-46.
30. Lowry CA, Cooper MJ. The problem of Compton scattering in emission tomography: A measurement of its spatial distribution. Phys Med Biol 1987;32:1187-91.
31. Zaidi H, Koral KF. Scatter modelling and compensation in emission tomography. Eur J Nucl Med Mol Imaging 2004;31:761-82.
32. Hamill JJ, DeVito RP. Scatter reduction with energy-weighted acquisition. IEEE Trans Nucl 1989;36:1334-9.
33. Halama JR, Henkin RE, Friend LE. Gamma camera radionuclide images: Improved contrast with energy-weighted acquisition. Radiology 1988;169:533-8.
34. DeVito RP, Hamill JJ, Treffert JD, Stoub EW. Energy-weighted acquisition of scintigraphic images using finite spatial filters. J Nucl Med 1989;30:2029-35.
35. Koral KF, Wang XQ, Rogers WL, Clinthorne NH, Wang XH. SPECT Compton-scattering correction by analysis of energy spectra. J Nucl Med 1988;29:195-202.
36. Gagnon D, Todd-Pokropek A, Arsenaault A, Dupras G. Introduction to holospectral imaging in nuclear medicine for scatter subtraction. IEEE Trans Med Imaging 1989;8:245-50.
37. Floyd CE Jr, Jaszczak RJ, Greer KL, Coleman RE. Inverse Monte Carlo as a unified reconstruction algorithm for ECT. J Nucl Med 1986;27:1577-85.
38. Floyd CE, Jaszczak RJ, Coleman RE. Inverse Monte-Carlo: A unified reconstruction algorithm for SPECT. lEEE Trans Nucl Sci 1985;32: 779-85.
39. Koral KF, Clinthorne NH, Rogers WL. Improving emission-computed-tomography quantification by Compton-scatter rejection through offset window. Nucl Inst Meths Phys 1986;242A: 610-4.
40. Khorshidi A, Ashoor M. Modulation transfer function assessment in parallel beam and fan beam collimators with square and cylindrical holes. Ann Nucl Med 2014;28:363-70.
41. Beck JW, Jaszczak RJ, Coleman RE. Analysis of SPECT including scatter and attenuation using sophisticated Monte-Carlo modeling methods. IEEE Trans Nucl Sci 1982;29: 506-11.
42. Kulkarni S, Khurd P, Zhou L, Gindi G. Statistical properties of SPECT MAP reconstruction incorporating window based scatter correction. Nucl Sci IEEE Trans 2009;56:97-107.
43. Ogawa K, Ichihara T, Kubo A. Accurate scatter correction in single photon emission CT. Ann Nucl Med Sci 1994;7:145-50.
44. Dewaraja Y, Li J, Koral K. Quantitative ^{131}I SPECT with triple energy window Compton scatter correction. IEEE Trans Nucl Sci 1998;45:3109-14.
45. Ritt P, Vija H, Hornegger J, Kuwert T. Absolute quantification in SPECT. Eur J Nucl Med Mol Imaging 2011;38:69-77.
46. Todd-Pokropek AE, Clarke G, Marsh R. Preprocessing of SPECT data as a precursor for attenuation correction. In: Deckonic F, editor. Information Processing in Medical Imaging. Bruxelles: Martinus Nijhoff Publishers; 1983. p. 130-50.
47. Msaki P, Axelsson B, Israelsson A, Larson SA. An Improved Scatter Correction Technique in SPECT Using Point Spread Scatter Function. Espoo, Finland: Presented at the International Conference on Medical Biology and Engineering and International Conference on Medical Physics; 1985.
48. Lowry CA, Taylor DN, Holt RS, Cooper MJ, McIntosh JA. Single Photon Emission Computed Tomography: Correction for Compton Scattered Photons. Coventry, England: Conference Abstracts, 43rd Annual Conference on HPA; 1986.
49. Egbert SD, May RS. An integral-transport method for Compton-scatter correction in emission computed tomography. Nucl Sci IEEE Trans 1980;27:543-8.

How to cite this article: Ashoor M, Asgari A, Khorshidi A, Rezaei A. Evaluation of Compton attenuation and photoelectric absorption coefficients by convolution of scattering and primary functions and counts ratio on energy spectra. Indian J Nucl Med 2015;30:239-47.

Source of Support: Nil. **Conflict of Interest:** None declared.